Research article

Zhanghua Han*, Fei Ding, Yangjian Cai and Uriel Levy

Significantly enhanced second-harmonic generations with all-dielectric antenna array working in the quasi-bound states in the continuum and excited by linearly polarized plane waves

https://doi.org/10.1515/nanoph-2020-0598
Received November 5, 2020; accepted November 26, 2020; published online December 4, 2020

Abstract: The recently emerging all-dielectric optical nanoantennas based on high-index semiconductors have proven to be an effective and low-loss alternative to metal-based plasmonic structures for light control and manipulations of light–matter interactions. Nonlinear optical effects have been widely investigated to employ the enhanced interactions between incident light and the dielectrics at the Mie-type resonances, and in particular magnetic dipole resonances, which are supported by the semiconductor. In this paper, we explore the novel phenomenon of bound states in the continuum supported by high-index semiconductor nanostructures. By carefully designing an array of nanodisk structures with an inner air slot as the defect, we show that a novel high quality-factor resonance achieved based on the concept of bound state in the continuum can be easily excited by the simplest linearly polarized plane wave at normal incidence. This resonance further enhances the interactions between light and semiconductors and boosts the nonlinear effects. Using AlGaAs as the nonlinear material, we demonstrate a significant increase in the second-harmonic generation efficiency, up to six orders of magnitude higher than that achieved by magnetic dipole resonances. In particular, a second-harmonic generation efficiency around 10% can be numerically achieved at a moderate incident pump intensity of 5 MW/cm^2.

Keywords: all-dielectric nanoantenna; bound state in the continuum; nonlinear applications; local field enhancement.

1 Introduction

The use of resonating artificial structures such as nanoantennas to control light–matter interactions has been the subject of intense and continuous research interest over the past several decades [1]. These enhanced interactions can support a variety of novel applications, including optical detection of weak signals [2, 3], controlled spontaneous emission [4] and strong coupling [5], to name a few. In the last decade, the use of optical nanostructures to enhance nonlinear optical effects has attracted ever growing attention, with the aim to mitigate or even free the requirement of phase matching conditions [6]. Due to the extremely low nonlinear susceptibility of most materials, optically thick nonlinear materials are conventionally required to achieve a considerable nonlinear generation, and a careful structural design is important so that the nonlinear signals generated along the propagation path of the pump laser can add up constructively to achieve a maximum output. This requirement restricts the occurrence of efficient nonlinear optical process at the nanoscale and the subsequent on-chip applications. To overcome this deficiency, nanostructures based on noble metals

***Corresponding author: Zhanghua Han**, Shandong Provincial Key Laboratory of Optics and Photonic Devices and Shandong Provincial Engineering and Technical Center of Light Manipulations, School of Physics and Electronics, Shandong Normal University, Jinan 250358, China, E-mail: zhan@sdnu.edu.cn. https://orcid.org/0000-0002-4177-2555
Fei Ding, Center of Nano-Optics, University of Southern Denmark, Campusvej 55, Odense M, Denmark. https://orcid.org/0000-0001-7362-519X
Yangjian Cai, Shandong Provincial Key Laboratory of Optics and Photonic Devices and Shandong Provincial Engineering and Technical Center of Light Manipulations, School of Physics and Electronics, Shandong Normal University, Jinan 250358, China
Uriel Levy, Department of Applied Physics, The Hebrew University of Jerusalem, Jerusalem, Israel

Open Access. © 2020 Zhanghua Han et al., published by De Gruyter. This work is licensed under the Creative Commons Attribution 4.0 International License.

which support localized surface plasmons allowing field confinement at the deep nanoscale alongside with moderately high values of surface second-order nonlinear susceptibility have been exploited [7, 8]. Different second-order nonlinear optical effects including second-harmonic generations (SHGs) [9–11], difference frequency generation (DFG) to realize continuous wave or even broadband terahertz pulses [12, 13] have been reported. The main drawback in the use of metallic nanostructures is still associated with the intrinsic loss with metals, which not only deteriorates the resonating properties and the local field enhancement capability, but also leads to a low damage threshold of pump laser density due to the absorption of energy. Later, all-dielectric nanoantennas supporting multipolar Mie resonances [14] and even more sophisticated modes like anapoles [15] have emerged as an effective alternative to the metallic counterpart in terms of nonlinear applications [16, 17]. In particular, the dielectric nanoantennas are made from high-index semiconductor materials with relatively high nonlinear susceptibilities and near-zero optical absorption at the pump wavelength, which make this approach even more promising. Enhanced SHG by the magnetic dipole (MD) resonances supported by AlGaAs individual nanodisks or arrays have been experimentally realized [18, 19]. The nonlinear conversion efficiency, defined as the power at the second harmonic (SH) frequency normalized by the pump power, have been reported at the order of 10^{-5} when the pump laser power intensity is at the GW/cm^2 level, which is roughly four order of magnitude higher compared to that from a bare AlGaAs film of the same thickness. However, the generated nonlinear power is still too low and far from being acceptable in practical applications.

Quite recently, researchers have stepped forward by predicting that the SHG efficiency can be further improved by additional two orders of magnitude as compared to pure MD resonance, by using the novel phenomenon of bound state in the continuum (BIC) [20] supported by isolated AlGaAs nanoantennas. BIC modes are formed due to destructive interference of two similar leaky modes, which cancel each other and the resonance manifests itself as a super-cavity mode with extremely large quality factors. SHG enhanced by BIC mode supported by a standard circular AlGaAs disk has recently been experimentally investigated [21], providing a verification to the theoretical prediction. For the AlGaAs disks investigated therein, the supported BIC mode has an azimuthal electric field distribution. As a result, one needs to use the complicated azimuthally polarized vector beam as the excitation.

2 Structure and results

In this work, we further explore the concept of BIC by using an AlGaAs nanoantenna array, which exhibits much higher quality factors and less requirement on the excitation condition based on a careful design of the structure. We show that by etching a narrow slot inside the disk, the quasi-BIC (QBIC) mode in the AlGaAs disk array can be easily excited by a simple plane wave with a linear polarization. When the slot is sufficiently small, its existence only works as a small perturbation to the AlGaAs disk mode. So the quality factor associated with the resonance supported by the slotted disk remains extremely high, and can be easily adjusted by the degree of symmetry-breaking depending on the position of the slot. Meanwhile, the slot can operate as a void antenna which can be easily excited with a linearly polarized wave. This way, the QBIC mode in the whole disk array can be subsequently activated. Thanks to the high quality factor of the QBIC mode and the associated high electric field enhancement, an incident wave at the resonance of the QBIC mode will have an extremely strong interaction with the AlGaAs disk array. Our investigations show that even with a relatively low pump intensity of 5 MW/cm^2, an efficient SHG with the efficiency around 10% can be numerically achieved.

The schematic concept is illustrated in Figure 1, where the red beam represents the incident wave at QBIC resonance and the purple beam below the structure is the generated SH signal. The whole structure consists of a

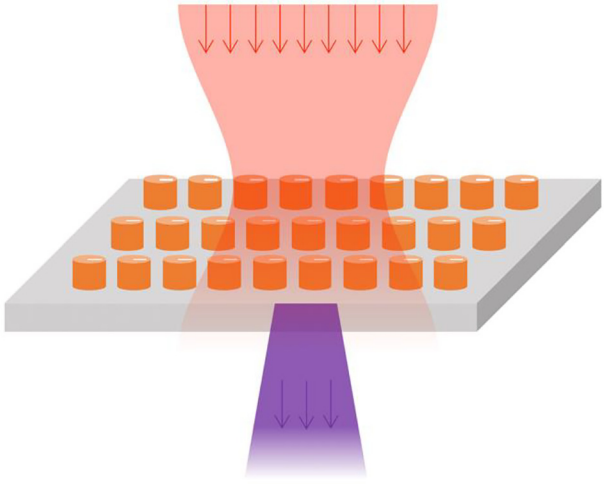

Figure 1: Schematic illustration of the second-harmonic generations (SHG) enhanced by the quasi-bound state in the continuum (QBIC) mode supported by slotted AlGaAs disk array. The red beam represents the incident wave at QBIC resonance while the outgoing purple beam is the generated second harmonic (SH) signal.

quartz substrate (index 1.444) with slotted AlGaAs disk array on top, whose top and cross-sectional views are shown as the inset in Figure 2(a). The radius and height of the disk are chosen as 200 and 450 nm, respectively, to support Mie resonances of both the electric and magnetic types in the near infrared. An air slot with the length $L = 150$ nm and width $W = 20$ nm is etched into the AlGaAs disk, while the center of the air slot is laterally shifted from the disk axis by a distance of D. The whole array is arranged in a square lattice with periodicity of $P = 900$ nm in both the x and y directions. We first set D to 20 nm and calculated the band structure of the slotted AlGaAs array by solving for the eigen resonance of the array using the finite-element method (FEM). Floquet periodic boundary conditions are used in the xy plane while perfectly matched layers are applied along the z direction. To simplify the computational effort, the refractive index of the AlGaAs and SiO_2 layers are set to 3.2 and 1.444 with no dispersion. Neglecting the material dispersion is valid when we are only interested in the narrow band BIC phenomenon. As is shown by the solid blue line in Figure 2(a), the slotted AlGaAs disk array supports a resonance which is well above the light line (shown as the dashed line). The relative position between the resonances and the light line show that the resonances supported by the slotted disk array indeed belongs to the category of BIC. The spectral position of the resonance is only weakly affected by the lateral wave vector, indicating that it can also be excited by an inclined incidence. The dependence of the resonance and the associated quality factor as a function of the deviation D between the two centers are shown in Figure 2(b). As can be seen, when D is 0 and the whole structure is symmetric, the quality-factor approaches infinite, representing the case of a perfect BIC mode, which, however, can be hardly excited due to its closed channel of coupling to the external sources. As D increases, the resonance wavelength is slightly decreasing. Although the slot is small and only has a perturbative effect, the shift in resonance indicates that a higher asymmetry of the slotted disk affects the phase condition of resonance. In contrast to the small effect on the resonance wavelength, the value of D has an enormous effect on the quality (Q) factor in the slotted disk. As is shown in Figure 2(b), the quality factor decreases substantially for a larger asymmetry, which, however, is still above a level of ~10^3 and much higher than those achieved for conventional Mie resonances in all-dielectric nanostructures [22]. We need to note that although a higher asymmetry leads to a slight deterioration of the Q factor, as we will show in the following part, the QBIC resonance can be easily excited in the slotted disk array using a linearly polarized plane wave. Clearly, when considering fabrication of such structures, e.g., by electron beam lithography (EBL), some misalignment error is expected, which is usually in the order of a few nanometers. In that case one can simply set D to 0 in the pattern design, the final structure will have a D values spread around few nanometers, all corresponding to a high quality-factor above 10^4, as indicated in Figure 2(b).

We further calculate the transmission spectrum through the slotted disk array using the FEM approach. Here the value of D is set to 20 nm, which, as we can see from Figure 2(b), leads to a resonance around 1.486 μm

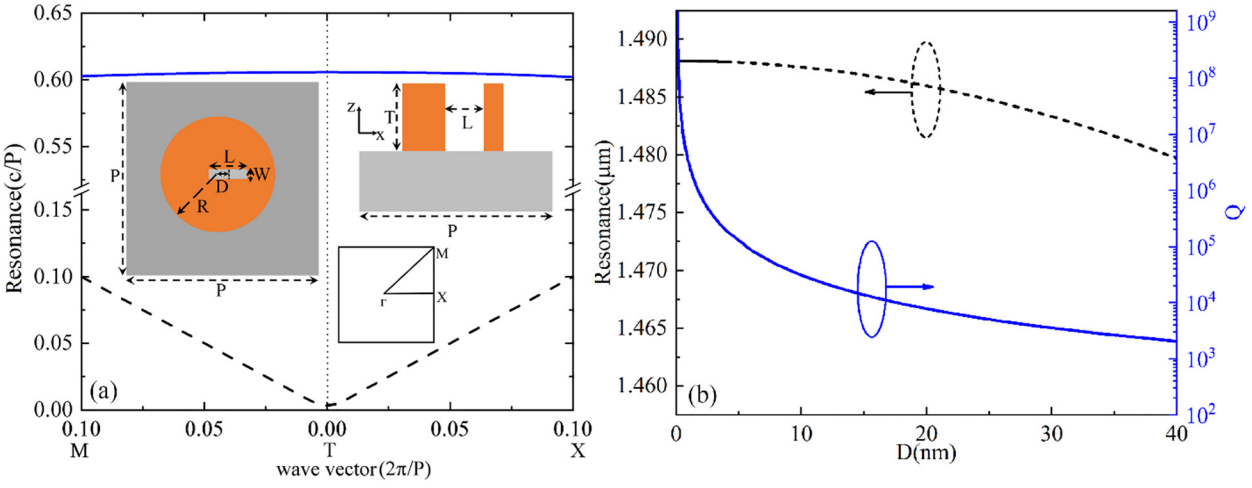

Figure 2: (a) band structure of the bound state in the continuum (BIC) mode supported by the slotted AlGaAs disk array. The blue line corresponds to the BIC mode and dashed line represents the light line. Inset: top (left) and cross-sectional (right) views of the single unit, where the air slot with length L and width W is etched through the AlGaAs disk. (b) Calculated eigen resonance of the associated quality factors supported by the slotted AlGaAs disk array, as a function of the relative position between the centers of the slot and the disk.

with a quality factor of about 8000. A linearly polarized plane wave with E field along y direction is incident normal to the array and transmittance as a function of incident wavelength is shown in Figure 3(a). Since the periodicity of array is 900 nm, the whole array works in the subwavelength regime when the wavelength is above 1300 nm and only zero-order transmission is present. From Figure 3(a), it can be seen that two resonances are present, one quite broad around 1.43 μm, while the other, around 1.4855 μm, is sharp with a strong Fano profile. Detailed calculations show that the broad resonance is due to the excitation of the magnetic dipole (MD) mode supported by the AlGaAs disk [23]. The electric dipole (ED) resonance is not observed in Figure 3(a) because it is outside of the spectral range. An enlarged figure of the sharp resonance is shown as the black dashed line in Figure 3(b), which shows more clearly the resonance bandwidth and its spectral position. The Fano profile is due to the interference between the broad MD mode and the sharp QBIC mode. We have also plotted in Figure 3(b), the maximum of the local electric field amplitude within the AlGaAs (excluding the air slot). As can be seen, a local electric field enhancement of ~190 is achieved by the QBIC resonance. This huge E field enhancement makes it possible to boost the light–matter interactions and nonlinearities at the nanoscale.

Our calculations (results not shown here) also indicate that a plane wave with x polarization cannot excite the sharp resonance. This polarization dependence is due to breaking of symmetry by the air slot. The magnetic field amplitude distribution (color coded) as well as the vectorial profile of the electric field (blue arrows) at the wavelength of the QBIC resonance is plotted in Figure 4(a). It is revealed about a right-handed rule between the E field circulation and the magnetic field (the magnetic field is along z direction while the electric fields are circulating within the xy plane). Furthermore, the E field inside the air slot is stronger than in the AlGaAs region, due to the permittivity contrast between AlGaAs and air, and the need for continuity of the electric displacement field. When the air slot is absent, this mode cannot be excited because both the electric and magnetic fields in the incident plane wave are normal to the corresponding component inside the AlGaAs disk, leading to a zero overlap. However, when the air slot is introduced, it operates as a void antenna and can be easily excited by the incident plane wave with proper polarization. As a result, the whole QBIC mode can be activated.

The relatively large second-order nonlinear susceptibility, $\chi^{(2)}$, of AlGaAs, alongside with the large local electric field enhancement shown in Figure 3(b), make the slotted AlGaAs disk array an ideal platform for efficient SHG at the nanoscale. Note that a quite high nonlinear generation may be expected, and in that case the incident wave at the fundamental frequency (FF) will be significantly affected by the SHG. So we abandoned the undepleted-pump approximation which is widely used in conventional nonlinear optics and switched to a more strict fully coupled approach. Thanks to the zinc-blend crystal structure of AlGaAs, its $\chi^{(2)}_{ijk}$ tensor is non-zero only when $i \neq j \neq k$. As a result, the propagation of electromagnetic waves at both the fundamental and the second harmonic frequencies can be simplified into a set of coupled equations in (1)–(4), where the numbers 1 and 2 represent the fundamental and the second harmonic frequency, respectively, and i, j, k

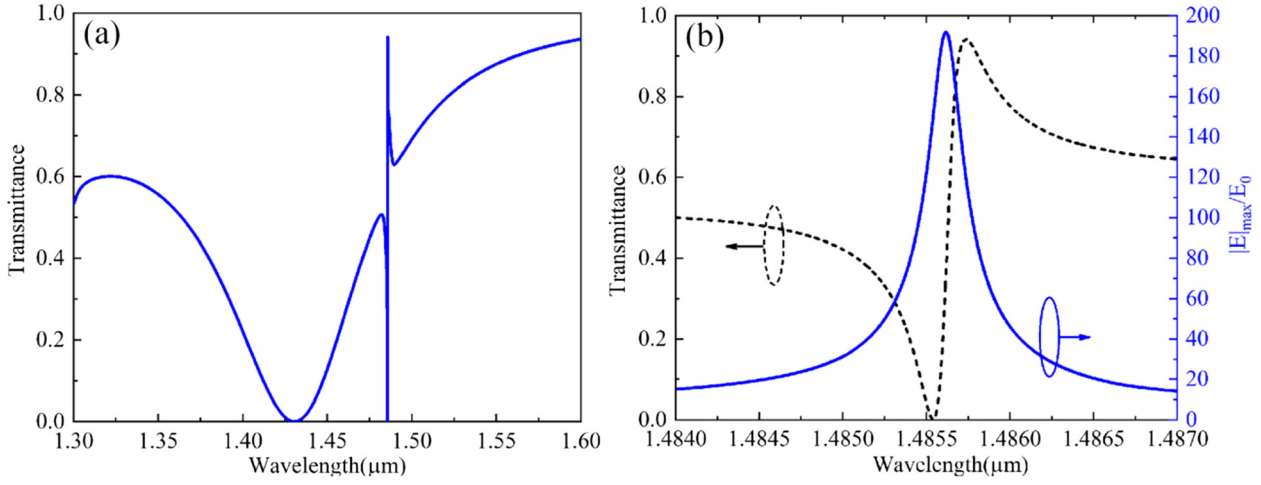

Figure 3: (a) Transmission spectrum through the slotted AlGaAs disk array with a linearly polarized plane wave excitation; (b) Zoom in showing the sharp resonance in (a), black dashed line. Also plotted in blue is the maximum of the local electric field amplitude in the AlGaAs domain as a function of wavelength.

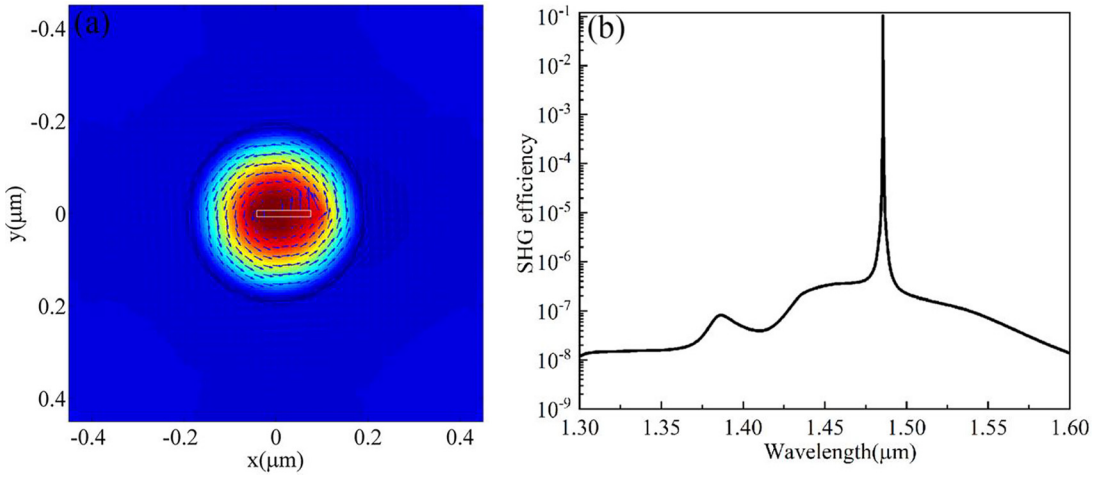

Figure 4: (a) Distribution of the magnetic field amplitude. Superimposed (blue arrows) is the vectorial orientation of the electric field inside the slotted disk at the wavelength of 1.4855 μm; (b) Calculated second-harmonic generations (SHGs) efficiency in the slotted AlGaAs disk array.

denotes the different components of the fields. The polarization at the SH frequency is due to the strong electric field at the FF, which works as an effective source to generate all the fields at SH based on equation (3). When the SHG is sufficiently strong, the electric field at the SH frequency will in return affect the polarization at the fundamental frequency by equation (2). As a consequence, the propagation at the fundamental frequency will be influenced. So in general, the calculation of the SHG in the slotted AlGaAs array needs to be solved by the following coupled equations:

$$\nabla \times \left(\nabla \times E_{1i}\left(\vec{r}\right)\right) - k_1^2 \epsilon_1\left(\vec{r}\right) E_{1i}\left(\vec{r}\right) = \omega_1^2 \epsilon_0 \mu_0 P_{1i} \quad (1)$$

$$P_{1i} = \sum \chi^{(2)} E_{2j}\left(\vec{r}\right) \cdot E_{1k}^{*}\left(\vec{r}\right) \quad (2)$$

$$\nabla \times \left(\nabla \times E_{2i}\left(\vec{r}\right)\right) - k_2^2 \epsilon_2\left(\vec{r}\right) E_{2i}\left(\vec{r}\right) = \omega_2^2 \epsilon_0 \mu_0 P_{2i} \quad (3)$$

$$P_{2i} = 0.5 \sum \chi^{(2)} E_{1j}\left(\vec{r}\right) \cdot E_{1k}\left(\vec{r}\right) \quad (4)$$

From the experimental results reported in the literature studies [18], it is known that the damage threshold of the incident pump laser intensity for the AlGaAs MD resonance is around the order of a few GW/cm^2. Actually the damage threshold should be determined by the intensity within the AlGaAs material, so one needs to take into account the local E field enhancement provided by the MD resonance and the much higher field enhancement that can be achieved by the QBIC resonance investigated here. Assuming I_d is the damage threshold of InGaAs material, f_1 and f_2 are the maximum local electric enhancement provided by the MD and QBIC resonances, respectively, I_1 and I_2 are the incident pump light intensity for the two resonances, then one can have:

$$I_d = f_1^2 I_1 = f_2^2 I_2 \quad (6)$$

Assuming typical values of $f_1 = 5$ and $I_1 = 8.1$ GW/cm^2 by the MD resonance [18, 19], and using the value of $f_2 = 190$ from Figure 3(b), one can calculate a value of I_2 to be 5.61 MW/cm^2. Therefore, we have chosen the pump laser intensity of the incident plane wave to be as low as 5 MW/cm^2, which, together with the results given in Figure 3(b), gives rise to a local intensity maximum close to, but still below the reported damage threshold of InGaAs. We define the SHG efficiency η as the power at the SH frequency emitted from the output port of the slotted disk array unit cell normalized to that at the fundamental frequency incident into the input port, i.e., $\eta = P_{\mathrm{SHG}}/(I_0 * P^2)$. The $\chi^{(2)}$ value of the AlGaAs material is set as 200 pm/V [19], which is a high value compared to most materials and is an advantage of AlGaAs for applications in nonlinear optics. With all the above assumptions, the FEM method implemented by the commercial software of Comsol Multiphysics is used to solve eqs. (1)–(4). The calculated SHG efficiency as a function the excitation wavelength is shown in Figure 4(b), which reveals that an unprecedented high efficiency above 10% can be achieved at the frequency of the QBIC mode. The MD resonance at 1.43 μm wavelength shown in Figure 3(a), which is also supported by the slotted disk structure, exhibits a significantly lower SHG efficiency, at the order of 10^{-7} at the same pump intensity. One can see that the QBIC resonance can enhance the SHG efficiency by a factor of 10^6 compared to that achieved MD resonance.

To verify the huge enhancement of the SHG obtained at the QBIC mode as compared to the SHG efficiency achieved by the MD resonance, we further calculate the transmission spectrum and the SHG efficiency for the AlGaAs disk array with the same geometrical parameters as those given in Figure 2(a) except that the air slot is absent. The results (Figure 5) exhibit a similar signature to that observed by the MD resonance of the slotted disk, albeit the transmission dip is slightly red shifted and is now centered around 1.475 μm. The slight shit of the MD resonance is due to the absence of the air slot and the subsequent increase of the optical path. The calculated SHG efficiency confirms that at the incident pump intensity of 5 MW/cm^2, the SHG efficiency is at the order of 10^{-7}, consistent with the results of Figure 4(b). This SHG efficiency is about two orders of magnitude lower than that reported in the literature simply because a much lower pump power intensity is used here for the purpose of comparison to the QBIC case. The slight spectral mismatch between the transmission dip at 1.475 μm and the SHG peak around 1.50 μm is attributed to the mode mismatch inside the AlGaAs disk array at the fundamental and SH frequencies [24]. The weaker peak in the SHG efficiency around 1.39 μm is also due to a resonance inside the AlGaAs disk at the SH frequency of this wavelength. The results of Figure 5, together with those shown in Figure 4(b), further confirms that the QBIC mode supported by the slotted AlGaAs disk array can indeed provide a SHG efficiency enhancement at the order of 10^6 compared to that from the MD resonance. This high enhancement is attributed to a larger local electric field enhancement associated with the QBIC compared to the MD resonance. Since the QBIC resonance can only be excited when the incident plane wave has a polarization perpendicular to the long side of the rectangular slot, it implies that the SHG efficiency is quite dependent on the direction of the incident wave polarization.

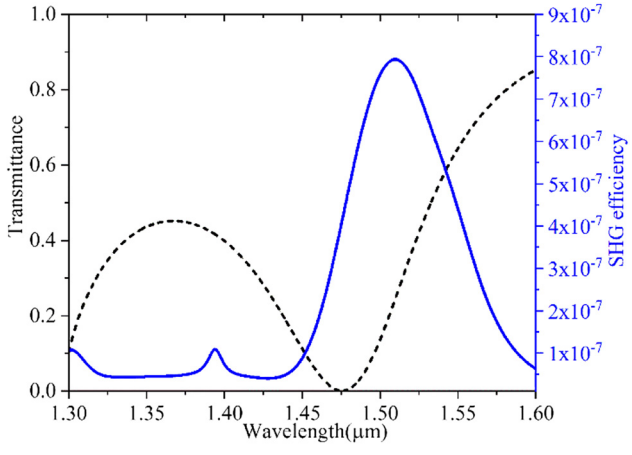

Figure 5: Transmission spectrum (dashed black line) and the second-harmonic generations (SHG) efficiency (blue line) from the magnetic dipole (MD) resonance supported by the AlGaAs disk array with no slot. Dimensions are similar to the slotted disk array.

3 Discussion

Our simulation results, assumes lossless AlGaAs material. In the real case, there might be some material absorption and scattering due to material and fabrication imperfections like roughness. At the same token, we also note that the lateral distance between the center of the air slot and the axis of the disk is chosen as 20 nm. From the results in Figure 2(b), one can see that the quality factor is quite sensitive to the degree of structural asymmetry, i.e., the value of D between the two centers. Since the local electric field enhancement is related with the resonance quality factor, the SHG efficiency will be affected by the degree of asymmetry significantly. For example, when the value of D increases from 20 to 40 nm, the quality factor of the QBIC resonance decreases from 7785 to 2043 and the calculated SHG efficiency at the pump wavelength of the corresponding QBIC resonance and the same incident pump intensity of 5 MW/cm^2 decreases from around 10 to 0.7%. In a realistic scenario, even with all the possible losses taken into account, we still believe that the BIC mode supported by the slotted AlGaAs disk array structure will exhibit a sharp resonance with a quality factor above 10^4, and that a high SHG efficiency, even not close to 10%, can still be expected considering the high enhancement of the SHG efficiency over the MD mode (cf. the results in Figures 4(c) and 5), which has already been experimentally demonstrated. The validation of these assumptions is left for experimental groups working in the field of nonlinear optics and metasurfaces, with access to AlGaAs technology.

Although similar approaches have been reported in the literature by introducing a defect, e.g., a hole [25], into the disk structure to break the symmetry, we note that our design, by using the rectangular slot, facilitates the excitation of the quasi-BIC mode for linearly polarized plane waves and then is preferable. Moreover, the local field inside the AlGaAs disk at the QBIC mode is much larger than that of the incident beam, and will easily lead to the breakdown of the material. However, to achieve the same SH power, a much lower pump laser power at the FF is required. As a result, the absolute efficiency of the SHG process is much higher.

Apart from the ease of excitation using a simple linearly polarized plane wave, another difference of our structure with isolated AlGaAs disks supporting similar QBIC modes [21] is that an array is used in our work while

isolated structures are adopted therein. The QBIC mode supported by the slotted disk array may have a much higher quality factor, which poses stringent requirement on the linewidth of the pump laser. However, we should note that the quality factor of QBIC in the slotted disk array can be adjusted by a large extent via controlling the dimension of air slot and the degree of asymmetry to cover the range between a few hundreds and up to be more than 10^4, suggesting more flexibility to use in practical applications.

4 Conclusion

In conclusion, we have investigated the QBIC mode which is provided by a slotted AlGaAs disk array structure. The resonating property of the BIC mode is shown to exhibit a sharp peak with a quality factor above 10^3, which can be further increased by reducing the structure asymmetry. With a moderate pump laser intensity of 5 MW/cm^2, a high SHG efficiency around 10% can be achieved, which is six orders of magnitude higher than that obtained by the MD resonance of a conventional disk. The use of moderate pump intensity is crucially important in practical applications, where considerations such as power consumption, size and price come into play. Furthermore, unlike the conventional MD mode, the QBIC mode can be simply excited by linearly polarized plane wave, without the need for complicated beam profiles and inclined illumination. As such, our findings, including both the high SHG efficiency and the ease of mode excitation, make this structure of slotted disk array an ideal platform for nonlinear optics at the nanoscale.

Acknowledgements: F. Ding acknowledges the support from VKR Foundation (Grant No. 00022988).
Author contributions: All the authors have accepted responsibility for the entire content of this submitted manuscript and approved submission.
Research funding: This work has been supported by the National Science Foundation of China (No. 11974221, 11525418, 91750201, 11974218).
Conflict of interest statement: The authors declare no conflicts of interest regarding this article.

References

[1] P. Biagioni, B. Hecht, J.-S. Huang, and B. Hecht, "Nanoantennas for visible and infrared radiation," *Rep. Prog. Phys.*, vol. 75, p. 024402, 2012.
[2] L. Tang, S. E. Kocabas, S. Latif, et al., "Nanometre-scale germanium photodetector enhanced by a near-infrared dipole antenna," *Nat. Photonics*, vol. 2, no. 4, pp. 226–229, 2008.
[3] M. W. Knight, H. Sobhani, P. Nordlander, and N. J. Halas, "Photodetection with active optical antennas," *Science*, vol. 332, no. 6030, pp. 702–704, 2011.
[4] M. S. Eggleston, K. Messer, L. Zhang, E. Yablonovitch, and M. C. Wu, "Optical antenna enhanced spontaneous emission," *Proc. Natl. Acad. Sci. USA*, vol. 112, no. 6, pp. 1704–1709, 2015.
[5] R. Chikkaraddy, B. De Nijs, F. Benz, et al., "Single-molecule strong coupling at room temperature in plasmonic nanocavities," *Nature*, vol. 535, no. 7610, pp. 127–130, 2016.
[6] M. Kauranen, "Freeing nonlinear optics from phase matching," *Science (80-)*, vol. 342, no. 6163, pp. 1182–1183, 2013.
[7] L. Novotny, N. Van Hulst, and N. van Hulst, "Antennas for light," *Nat. Photonics*, vol. 5, no. 2, pp. 83–90, 2011.
[8] J. A. Schuller, E. S. Barnard, W. Cai, Y. C. Jun, J. S. White, and M. L. Brongersma, "Plasmonics for extreme light concentration and manipulation," *Nat. Mater.*, vol. 9, no. 3, pp. 193–204, 2010.
[9] M. W. Klein, "Second-harmonic generation from magnetic metamaterials," *Science (80-)*, vol. 313, no. 5786, pp. 502–504, 2006.
[10] M. W. Klein, M. Wegener, D. Karlsruhe, N. Feth, and S. Linden, "Experiments on second- and third-harmonic generation from magnetic metamaterials," *Opt. Express*, vol. 15, no. 8, pp. 5238–5247, 2007.
[11] N. Segal, S. Keren-Zur, N. Hendler, and T. Ellenbogen, "Controlling light with metamaterial-based nonlinear photonic crystals," *Nat. Photonics*, vol. 9, no. 3, pp. 180–184, 2015.
[12] L. Luo, I. Chatzakis, J. Wang, et al., "Broadband terahertz generation from metamaterials," *Nat. Commun.*, vol. 5, pp. 1–6, 2014.
[13] D. K. Polyushkin, E. Hendry, E. K. Stone, and W. L. Barnes, "THz generation from plasmonic nanoparticle arrays," *Nano Lett.*, vol. 11, no. 11, pp. 4718–4724, 2011.
[14] Y. S. Kivshar, B. Luk, A. I. Kuznetsov, et al., "Optically resonant dielectric nanostructures," *Science (80-)*, vol. 354, no. 6314, p. aag472, 2016.
[15] A. E. Miroshnichenko, A. B. Evlyukhin, Y. F. Yu, et al., "Nonradiating anapole modes in dielectric nanoparticles," *Nat. Commun.*, vol. 6, pp. 1–8, 2015.
[16] B. Sain, C. Meier, and T. Zentgraf, "Nonlinear optics in all-dielectric nanoantennas and metasurfaces: a review," *Adv. Photonics*, vol. 1, no. 02, p. 024002, 2019.
[17] J. Bar-David and U. Levy, "Nonlinear diffraction in asymmetric dielectric metasurfaces," *Nano Lett.*, vol. 19, no. 2, pp. 1044–1051, 2019.
[18] S. Liu, M. B. Sinclair, S. Saravi, et al., "Resonantly enhanced second-harmonic generation using III–V semiconductor all-dielectric metasurfaces," *Nano Lett.*, vol. 16, no. 9, pp. 5426–5432, 2016.
[19] V. F. Gili, L. Carletti, A. Locatelli, et al., "Monolithic AlGaAs second-harmonic nanoantennas," *Opt. Express*, vol. 24, no. 14, p. 15965, 2016.
[20] L. Carletti, K. Koshelev, C. De Angelis, et al., "Giant nonlinear response at the nanoscale driven by bound states in the continuum," *Phys. Rev. Lett.*, vol. 121, no. 3, p. 33903, 2018.
[21] K. Koshelev, S. Kruk, E. Melik-Gaykazyan, et al., "Subwavelength dielectric resonators for nonlinear nanophotonics," *Science (80-)*, vol. 367, no. 6475, pp. 288–292, 2020.

[22] D. G. Baranov, D. A. Zuev, S. I. Lepeshov, et al., "All-dielectric nanophotonics: the quest for better materials and fabrication techniques," *Optica*, vol. 4, no. 7, p. 814, 2017.
[23] Z. Han, H. Jiang, Z. Tan, J. Cao, and Y. Cai, "Symmetry-broken silicon disk array as an efficient terahertz switch working with ultra-low optical pump power," *Chin. Phys. B*, vol. 29, no. 8, p. 084209, 2020.
[24] L. Carletti, A. Locatelli, O. Stepanenko, G. Leo, and C. De Angelis, "Enhanced second-harmonic generation from magnetic resonance in AlGaAs nanoantennas," *Opt. Express*, vol. 23, no. 20, pp. 26544–26550, 2015.
[25] K. Koshelev, S. Lepeshov, M. Liu, A. Bogdanov, and Y. Kivshar, "Asymmetric metasurfaces with high-Q resonances governed by bound states in the continuum," *Phys. Rev. Lett.*, vol. 121, no. 19, p. 193903, 2018.